energies

MDPI

Article

Prediction of Pressure Increase during Waste Water Injection to Prevent Seismic Events

Lu Jin [1,*], Andrew K. Wojtanowicz [1] and Jun Ge [2]

[1] Craft & Hawkins Department of Petroleum Engineering, Louisiana State University, Baton Rouge, LA 70803, USA; awojtan@lsu.edu
[2] Bureau of Economic Geology, The University of Texas at Austin, Austin, TX 78712, USA; jun.ge@beg.utexas.edu
* Correspondence: lujin329@yahoo.com

Abstract: A considerable increase of seismicity has occurred in the USA in the last decade (2009–2020) with an annual average of 345 M3+ earthquakes. Numerous field cases have shown that excessive well pressure due to a high injection rate may have triggered seismic events. This study defines conditions for inducing a seismic event by excessive injection in the well's pressure that may cause geomechanical damage to the rock. Introduced here is an analytical model and method for predicting pressure increase during injection of produced water contaminated with oil. The model calculates time-dependent advancement of the captured oil saturation causing the well's injectivity damage and pressure increase. Critical conditions for a seismic event are set by defining rock failure when well pressure exceeds the fracturing pressure of the wellbore or when the increased pore pressure reduces the effective normal stress at the "weak" interface inside the rock, computed with a geomechanical model. This concept is demonstrated in three field case studies using data from geological formations in areas of petroleum operations. The results confirm field observations of the initial rapid increase of oil invasion and injection pressure that could only be controlled by reducing the rate of injection to assure continuing long-time operation.

Keywords: injection wells; induced seismicity; produced water injection; injection pressure model; rock slippage diagram

Citation: Jin, L.; Wojtanowicz, A.K.; Ge, J. Prediction of Pressure Increase during Waste Water Injection to Prevent Seismic Events. *Energies* **2022**, *15*, 2101. https://doi.org/10.3390/en15062101

Academic Editors: Nediljka Gaurina-Međimurec and Borivoje Pašić

Received: 31 December 2021
Accepted: 11 March 2022
Published: 13 March 2022

1. Introduction

In the United States, the estimated volume of water produced in oilfields is in the range of 20 to 30 billion barrels (3.2–4.8 billion m^3) per year [1,2]. The volume has increased over the last decade due to maturing of conventional oil/gas fields and the development of unconventional shale deposits [3–5]. In 2020, approximately 65% of the total oil production in the US was from unconventional reservoirs as reported by the U.S. Energy Information Administration (US EIA). Table 1 shows the effect of the "shale revolution" on US water production [2].

Table 1. Comparison of oil, gas, and water production in the US before (2007) and after (2017) the "shale revolution" [2].

Time	Category		
	Oil, Million bbl/yr (Million m^3/yr)	Gas, Million cf/yr (Million m^3/yr)	Water, Million bbl/yr (Million m^3/yr)
2007	1750 (278)	24,374,000 (69,016)	20,195 (3211)
2012	2264 (360)	29,730,220 (841,868)	21,181 (3368)
2017	3405 (541)	35,005,078 (991,235)	24,395 (3878)

For unconventional reservoirs, the quantity of water used for hydraulic fracturing could vary from 10,000 to 24,000 m^3 per well (per the U.S. Environmental Protection Agency, US EPA) [6]. After fracturing most of the injected water usually flows back to the surface and the flow back water is typically injected into the subsurface with injection wells. (Although a variety of methods including surface discharge, evaporation, offsite commercial disposal, and beneficial reuse, etc. have been used to manage the produced water associated with oil and gas production, the deep-well injection has been the main technology for managing most of the produced wastewater for decades [7–9].) The hydraulic fracturing process has created a new demand for wastewater disposal wells that inject waste fluids into deep geologic formations [10].

It was observed that increasing volumes of wastewater injection correlate with an increasing rate of seismic activity [11–13]. Figure 1 demonstrates a series of seismic events in Oklahoma, Texas, New Mexico and Arkansas, etc. where most of these events in recent years have been related to wastewater disposal associated with oil and gas production, especially with the boom of unconventional resources [14]. In Oklahoma alone, more than 20 earthquakes of magnitudes 4.0 to 4.8 occurred since 2009, which include the largest earthquake in the state's history (magnitude 5.7) that occurred on 6 November 2011, near Prague, causing damage to several structures nearby [11]. The number of earthquakes with a magnitude exceeding M3.0 (magnitude 3.0) has increased dramatically since 2009: from approximately 20/year between 1970 and 2000 to over 100/year between 2010 and 2013, even exceeding 500/year between 2014 and 2016. The rate peaked in 2015 with 1010 M3+ earthquakes. Although the rate has declined since 2015, there were still 130 M3+ earthquakes recorded in the same region in 2019. Some of them were particularly strong and damaging such as the M5.8 Pawnee and M5.0 Cushing Oklahoma earthquakes that occurred in 2016 [15–17].

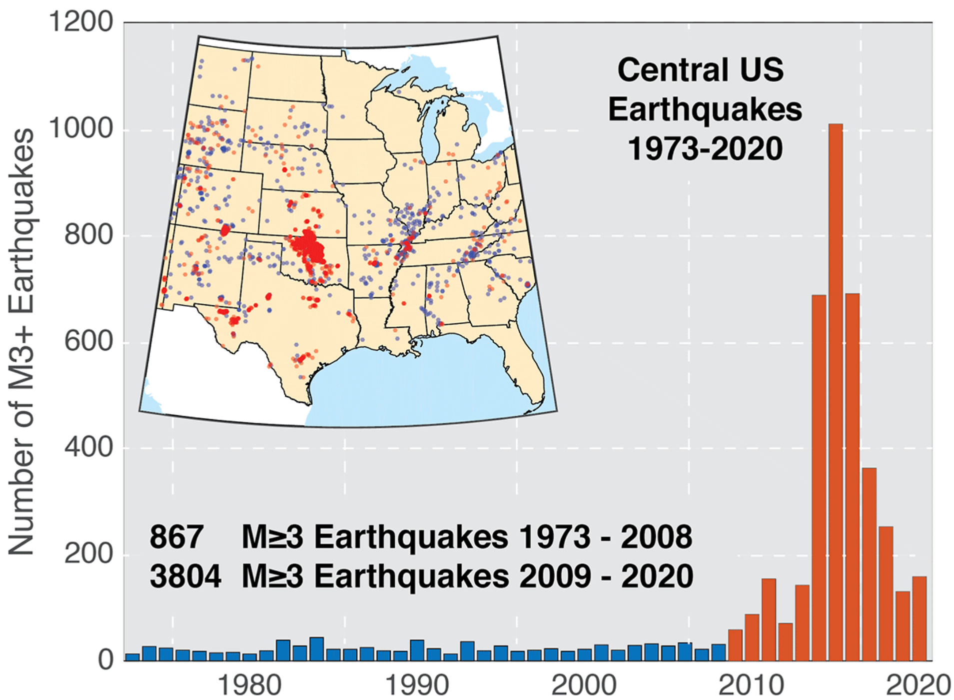

Figure 1. Increase of M3+ earthquakes in the central U. S. (USGS, 2021) [15].

A causal relationship between water injection and seismicity has been also suggested. Peña Castro et al. [11] reported a field case of water disposal-induced earthquakes in Northern Oklahoma and its analogy to the M7.8 Ecuador earthquake (in 2016) resulting from subsurface stress change due to water injection. In addition, Frohlich analyzed data collected by a network of temporary seismographs deployed under the EarthScope USArray program in the Barnett Shale oilfield operations between November 2009 and September 2011 [18]. (The seismographs recorded strength and location of regional earthquakes larger than M1.5.) He identified 67 earthquakes and located 24 epicenters in areas with one or more injection wells.

Despite increasing evidence, a causal relationship between seismic events and wastewater injection parameters (such as water quality, injection rate, and duration, etc.) is still not entirely proven and is a subject of pending research studies. For example, only a small fraction of the more than 30,000 U.S. wastewater disposal wells appears to be associated with damaging earthquakes [19]. Field experience, however, has shown that when produced water is injected into a deep formation the operation is hampered by a loss of injectivity due to permeability impairment caused by the low quality of the water, which in turn leads to an increase in injection pressure that may cause the formation failure such as fracturing and interlayer or fault slippage [20].

Traditionally, in the USA, subsurface injection of produced water is regulated by the Underground Injection Control (UIC) program of the Safe Drinking Water Act (SDWA) administered by the Federal Government and the States [21]. Produced water injection wells are classified as Class II wells and authorized by technical permit focused on the protection of subsurface aquifers—Underground Sources of Drinking Water (USDW). The protection clause sets a requirement for the maximum injection pressure that would prevent the injected wastewater from breaking from the injection zone upwards to USDW. The computations require geological data on the depths and distance from the well to USDW and, particularly, identification of faults or dipping formations that could become a pathway for moving the injected wastewater to USDW. However, the regulations do not address another environmental concern resulting from the state of stresses in the injection zone that controls its fracture resistance and the presence of faults and lithological structures with pre-stressed "weak interfaces" that could slip against each other—All being a potential source of a seismic event.

2. Research Gaps and Objectives

Numerous studies investigated the slippage potential of faults and fractures in different ways, including analytical calculation, numerical simulation, and semi-analytical methods [22–24]. Most studies rely on the understanding of both the geological and mechanical properties of the faults and fractures in the formations. Fractures with different orientations can be theoretically expected for different slip regimes. As pointed out by Dvory and Zoback [25], stress conditions including orientation and magnitude can vary at different scales, which is also critical to the fault slip potential analysis. Therefore, both rock fracturing failure and slip failure due to water injection are investigated in this study.

Pressure increase during fluid injection has been actively investigated in recent decades in response to increased oilfield production and growing demand for environmentally safe operation [26]. Mathias et al. conducted a series of modeling studies to predict pressure buildup in geologic formations for different boundary conditions [27,28]. Noirot et al. demonstrated injection-related rock fracturing using downhole microseismic data from water disposal wells in deep geologic formations. They developed analytical and numerical models to investigate the interaction between pressure buildup and mechanical integrity of the host formation and caprock [29]. Using numerical simulation models, they designed a safe injection process by considering the acceptable limit of injection pressure increase due to caprock integrity and formation fracturing. Lyu et al. studied the factors that control the water injection pressure to prevent rapid water breakthrough in the water flooding process when there are natural fractures in the reservoir [30]. They developed a model to determine the limit of water injection pressure based on the opening pressure of natural fractures in fractured low-permeability reservoirs. Abbaszadeh and Kamal studied the water injection performance in numerous waterflooding projects [31]. They examined a two-bank system with a step-change in saturation to consider the oil-water two-phase flow during the injection process and then developed a method to calculate the pressure behavior around an injector with a region of variable saturations. Their method was successfully applied to test water injectors in waterflooding operations. All of the above studies showed that injection rate and near-wellbore pressure buildup should be carefully designed especially by considering the geomechanical integrity of the host formation. However, they did not consider the effect and fate of oil contamination in the injected water.

Coulibaly and Borden's study admits that the injection rate-pressure behavior becomes more complex when there are oil droplets in the injection water since the oil droplets could form an in situ permeable reactive barrier in the near-well region [32]. As reported by Khan et al. and Kondash et al. [33], in unconventional plays, oil concentration in produced water may considerably vary—from 100 to 2000 ppm depending on the oil properties. Although produced water is somewhat cleaned by removing the oil before subsurface disposal, the injection of diluted oil/water mixture cannot be avoided as small oil droplets suspended in water are difficult to remove. After the separation, a small oil concentration (50~500 ppm) remains in the water to be injected into the host formation [34]. Injectivity decline is commonly encountered in such operations, especially when raw produced water is injected from wells with downhole oil-water separation, DOWS [35]. Field cases showed that instant injectivity damage occurs when untreated produced water is injected and the damage stabilizes with continuing injection [36]. It was also found that even very small oil concentrations, as low as 100 ppm, could build a 10% residual oil bank around the wellbore and reduce well injectivity by more than 70% [34,37]. Such a considerable reduction of injectivity would lead to high bottomhole pressure around the well and cause rock failure by fracturing or slippage at the rock's weak interfaces (faults, joints, interlayers, etc.) [11,18].

In conclusion, the literature survey shows that most of the studies, to date, have not quantified the effect of oil droplets in the injection water on the potential rock failure resulting from local formation pressure increase due to oil deposition. Two-phase flow of the oil/water mixture and capillary pressure contrast between oil and water control oil deposition would damage rock permeability causing pressure increase. Most of the injection well pressure models assume either linear flow or need complex numerical algorithms/software tools to predict well's pressure increase. This creates chellanges for operators to use the models to evaluate the potential risk caused by wastewater injection in their fields.

Therefore, the objective of this study is to develop an analytical model which can be used by operators to predict (1) the injection pressure increase during the PWRI process (resulting from oil saturation advancement and formation permeability damage), and (2) assess the environmental risk of long-term injection of a large volume of produced water by coupling the well pressure with geo-mechanical criteria for injection pressure-induced seismicity.

3. Research Methodology

We begin with the formulation of a hypothetical mechanism of injection-caused seismicity by showing the relationship between the injection well's hydraulics–bottomhole pressure, and the host rock's geomechanics–rock failure stress criteria. Then, we quantify the hydraulics by explaining why oil droplets in the injection water can lead to rapid injection pressure increase in the near-wellbore region. We introduce an analytical model for water injectivity decline and pressure increase in the radial flow regime based on the fundamental mechanisms. (To make the model easier to use in field practices, the injectivity decline model is then transformed into a skin factor correlation, which predicts dynamic flow behavior during the water injection process.) Finally, we quantify the geomechanics by introducing a method for finding critical conditions for a seismic event resulting from the loss of geostatic stress balance inside the host rock receiving the injected water.

3.1. Mechanisms of Injection-Caused Seismicity

Although earthquakes can be induced in many ways such as the filling up subsurface reservoirs, oil and gas production, fluid injection, mining, geothermal energy extraction, and other operations, each of these activities fundamentally causes earthquakes due to the same mechanism: a sudden release of stored elastic strain energy by frictional sliding along preexisting faults due to the change of their stress conditions [14]. Observations and numerical modeling showed that increased fluid pressure within faults is the main risk factor whether injection well will trigger earthquakes [12–18]. A case history of injection-induced seismicity demonstrated that elevating the pore pressure by hundreds of psi could cause a previously quiescent area to become seismically active when the regions are sufficiently prestressed [13,38]. Field cases showed that some earthquakes could be triggered far away from the injector after years of injection, while others were observed close to the injector shortly after the injection began. Depending on the distance between the injector and fault, it may take more time for the fault to be activated by pressure from a distant injector, while a close injector may promptly cause rock failure in the fault since most pressure increase usually occurs close to the well and it can effectively change the stress conditions in the nearby fault. Therefore, earthquakes could be triggered by two types of rock failure: (1) Type I—the pore pressure exceeds the fracturing pressure of the formation when the injection well is close to a fault, the fractures then cause fault failure and induce earthquakes. In this case, we need to ensure the maximum pore pressure around the injector be below the formation fracturing pressure to prevent rock failure and seismic events, while the maximum pressure is the bottomhole injection pressure in the water injection process; (2) Type II—the pore pressure exceeds the critical pressure that causes shear failure along with a strained "weak" interface inside the rock. The slippage, fracture (or both) would occur with an increase of pore pressure that reduces the effective normal stress at the interface and results in shear failure.

Obviously, not all high-pressure injection wells trigger earthquakes. The forces responsible for releasing the accumulated elastic strain energy in the rock should first raise the existing state of stress to a near-critical level, i.e., shear failure of the rock. Therefore, seismic events induced by fluid injection may not generate sufficient strain energy for release in earthquakes but may act locally to reduce the effective frictional strength of faults and, therefore, trigger earthquakes in areas where the state of stress and the accumulated elastic strain energy are already near-critical levels during natural geologic and tectonic processes. The Mohr-Coulomb model is the most common method for evaluating the shear failure of the rock induced by increasing the pore pressure [13]. Using a compression-positive convention, we assume that the onset of a seismic event resulting from slippage within the rock's structure (fault or interlayer surface) is adequately described by the friction criterion:

$$\tau_{crit} = \tau_0 + \mu_f(\sigma_n - p) \tag{1}$$

where τ_{crit} is the critical shear stress required to cause slippage of the fault; τ_0 is the inherent shear strength of the fault; μ_f is the coefficient of friction; σ_n is the normal stress acting across the fault; p is the pore pressure. Figure 2 shows the principle of Mohr-Coulomb stress analysis on a fault, where σ_1 and σ_3 are the maximum and minimum principal stresses on the fault, respectively; τ is the shear stress on the fault; C is the location of Mohr circle; R is the radius of the Mohr circle. Fault failure may happen when the Mohr circle intersects with the shear stress line shown in Figure 2b.

Two parameters defining the strength of the slippage interface can be calculated as,

$$C = \frac{\sigma_1 + \sigma_3}{2} \tag{2}$$

$$R = \frac{\sigma_1 - \sigma_3}{2} \tag{3}$$

When water was injected to the formation comprising weak interface pore pressure would increase thus reducing the maximum and minimum principal stresses at the interface as,

$$\begin{cases} \sigma_{1\_i} = \sigma_1 - p \\ \sigma_{3\_i} = \sigma_3 - p \end{cases} \tag{4}$$

where σ_{1_i} and σ_{3_i} are the reduced maximum and minimum principal stresses at the interface. Thus, the corrected values of the parameters are,

$$C_i = \frac{\sigma_1 + \sigma_3 - 2p}{2} \tag{5}$$

$$R_i = \frac{\sigma_1 - \sigma_3}{2} \tag{6}$$

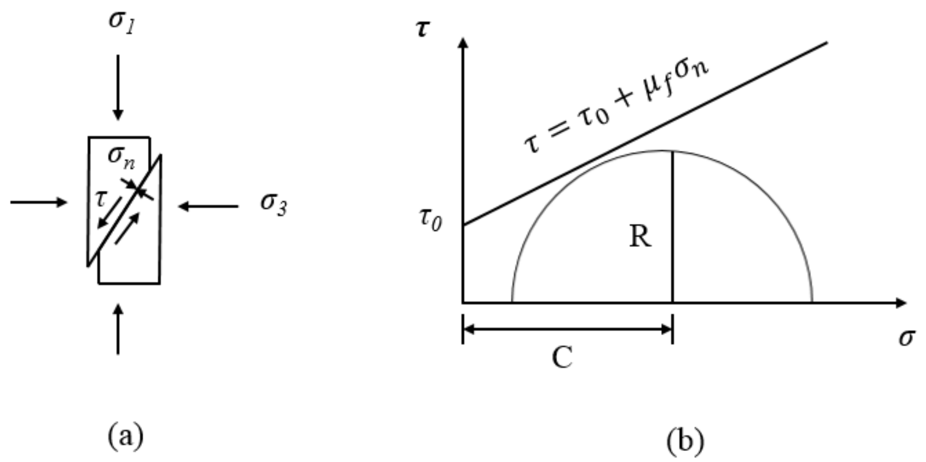

Figure 2. Principle of Mohr-Coulomb stress analysis of rock slippage: (**a**) Balace of of stresses; (**b**) Mohr-Coulomb failure criterion.

Although the radius of the Mohr circle in Figure 2b is not affected by the pore pressure increase, the circle moves leftwards thus meeting the shear failure conditions of Equation (1) and initiating slippage at the interface. When injectors are close to the weak planes in the rock structure the pore pressure in the rock may increase quickly with increasing injection pressure. That is why the injection well's hydraulics combined with geomechanics could describe the critical condition for inciting seismic events. Field observations show that injection pressure increases rapidly at the beginning of injection especially when there are oil droplets in the injection water. Sections 3.2 and 3.3 focus on developing an analytical model to predict the injection pressure increase due to oily water injection. Section 3.4 introduces a geomechanical model to predict slip rock failure in the injection process.

3.2. Analytical Modeling of Injectivity Decline

Most of the deep injectors in seismically active areas, such as Oklahoma and Texas, are used to inject produced water from oil and gas extraction activities, especially with the boom of unconventional resources development since 2009. Situations become complex when injecting wastewater back into unconventional reservoirs due to the extremely tight rock matrix and tiny pore throats (in nanometer-level), these tiny pore throats will create a high capillary resistance which prevents water from penetrating the matrix, instead, the injected water may flow to offset wells through fractures and reduce the productivity in these wells. Additionally, most of the unconventional reservoirs are still in the primary depletion stage, thus, water flooding has not been widely considered for (IOR) operations currently, instead, most of the produced water from unconventional reservoirs was injected into conventional formations for disposal.

Produced water in oilfields usually contains a certain amount of oil in four different types based on droplet size: free oil, dispersed oil, emulsified oil, and soluble oil [39]. Both experimental and theoretical work has shown that all four types of oil can cause severe formation damage around injectors by oil droplet capture, especially when there is no oil saturation in the formation at the beginning of injection [40]. The water permeability damage caused by oil droplets invasion is believed to relate to the following process: oil droplets are captured by rock matrix leading to an increase of oil saturation in the formation, which reduces the relative permeability of water, and water injectivity is impaired [37]. The loss of water injectivity causes a rapid increase of injection pressure in the near-wellbore region. If there is a fault in this impacted region, it may slip due to this high injection pressure.

Soo et al. conducted a series of experimental and theoretical works to study the emulsion flow in porous media. They identified two mechanisms for oil droplets capture in the rock: straining, where oil droplets clog the pore throats, and an interception—with droplets captured by van der Waals colloidal forces, etc. [41,42]. The injectivity decline model developed in this study considers the oil capture process as instant retention inside the rock that is controlled only by the size of the rock-fluid interface and concentration of oil in water. Similar to linear flow, oil droplets are transported by advection and dispersion, captured by adsorption in radial flow. The following assumptions are made to derive the mathematical expressions of the oily water injection process [43,44]:

1. The rock is homogeneous and no fines migration happens in the injection process;
2. The oil droplets and pore throats are log-normally distributed;
3. Oil droplet is the only contaminant, there are no solid particles in the injection water;
4. Oil droplets are stable and their sizes are constant in the water before being injected into the rock;
5. The oily water is injected into the rock at a constant flow rate;
6. No oil is generated or disappeared in the process.

Using cylindrical coordinate shown in Figure 3, oil transport in the porous media can be expressed as [4,40]:

$$\text{Advective mass flux rate} = \frac{\partial}{\partial r}(Cu_r\Delta\theta\Delta z\phi)\Delta r$$

$$\text{Dispersive mass flux rate (Fick's Law)} = -\frac{\partial}{\partial r}\left(D_r\frac{\partial C}{\partial r}\Delta\theta\Delta z\phi\right)\Delta r$$

$$\text{Rate of capturing by adsorption (Langmuir Adsorption): } \frac{\partial S_o}{\partial t} = \alpha\left(1-\frac{S_o}{S_{oe}}\right)C$$

where u_r is the interstitial water velocity in r direction, m/s; $\Delta\theta$, Δz, Δr are the arc length, height and radius of the controlled volume as shown in Figure 3, respectively, m; D_r is the overall dispersive coefficient which represents the strength of dispersion in the porous media, m^2/s. In contrast to bulk fluid flow in the formation, more fundamental details need to be considered for the flow of oil droplets. Dispersion is an important factor to characterize the flowing dynamics of small droplets, it is the macroscopic outcome of the actual movement of an individual oil droplet through the pores where various physical and chemical phenomena take place [45–47]. In actual reservoirs, Lake pointed out that dispersion is the mixing of oil and water caused by diffusion, local velocity gradients, and mechanical mixing in pore bodies [46]. The dispersive coefficient represents the rate of oil-in-water mixing-the larger the coefficient, the faster the mixing, and it is a function of velocity: $D_r = du_r$ where d is a constant referred as dispersivity, which is a measurement of heterogeneity of the porous media, m. In actual injection operations, the dispersive coefficient decreases with injection distance following the reduction of velocity in radial flow.

The mass balance equation for the oil phase can be expressed in the following equation since there is no oil generated or disappeared in the injection process:

$$\frac{\partial C}{\partial t}\Delta r\Delta\theta\Delta z\phi + \frac{\partial S_o}{\partial t}(1-\phi)\Delta r\Delta\theta\Delta z = \frac{\partial}{\partial r}\left(\frac{\partial C}{\partial r}du_r\Delta\theta\Delta z\phi\right)\Delta r - \frac{\partial}{\partial r}(Cu_r\Delta\theta\Delta z\phi)\Delta r \tag{7}$$

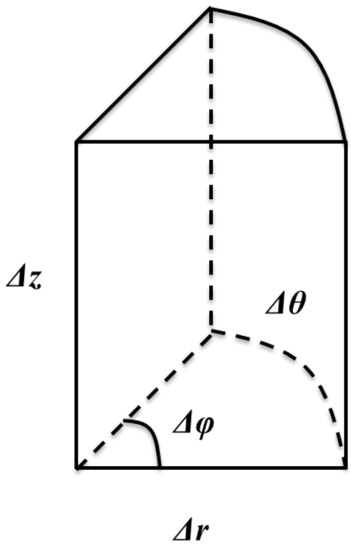

Figure 3. Controlled volume in cylindrical coordinate.

The following initial and boundary conditions can be used to solve Equation (7):
Initial condition, there is no oil in the formation before injection:

$$S_o = C = 0 \qquad at \;\; t = 0, \qquad r > r_w \tag{8}$$

Inner boundary condition, oil concentration is constant in the injection water before entering the formation:

$$C = C_0 \qquad at \;\; t > 0, \qquad r = r_w \tag{9}$$

Outer boundary condition, there is no oil in the formation at infinite length:

$$S_o = C = 0 \qquad at \;\; t > 0, \qquad r \to \infty \tag{10}$$

Solving Equations (10)–(13), we can obtain the oil concentration and saturation in the water and formation, respectively:

$$C = \frac{C_0 erfc\left(\frac{\frac{r^2}{2} - \frac{qt}{2\pi h_w \phi \varepsilon}}{\sqrt{\frac{4}{3} dr^3}}\right)}{erfc\left(\frac{\frac{r_w^2}{2} - \frac{qt}{2\pi h_w \phi \varepsilon}}{\sqrt{\frac{4}{3} dr_w^3}}\right)} \tag{11}$$

$$S_o = \frac{\alpha S_{oe} C_0 erfc\left(\frac{\frac{r^2}{2} - \frac{qt}{2\pi h_w \phi \varepsilon}}{\sqrt{\frac{4}{3} dr^3}}\right)}{\rho_o \left[erfc\left(\frac{\frac{r_w^2}{2} - \frac{qt}{2\pi h_w \phi \varepsilon}}{\sqrt{\frac{4}{3} dr_w^3}}\right) + \alpha C_0 erfc\left(\frac{\frac{r^2}{2} - \frac{qt}{2\pi h_w \phi \varepsilon}}{\sqrt{\frac{4}{3} dr^3}}\right)\right]} \tag{12}$$

$$\varepsilon = 1 + \frac{\beta(1 - \phi)}{\phi} \tag{13}$$

For oily water flowing through the formation, the change of permeability and pressure drop could be discretely depicted as shown in Figure 4. In such a case, we may compute a series of permeabilities in the rock sections as shown in the following equation:

$$K_{w\_avg} = \frac{10^6 q \mu_w ln \frac{r_e}{r_w}}{2\pi h_w} \frac{1}{\sum_{i=1}^{n} \Delta p_i} \tag{14}$$

where r_w and r_e are the radii of well and aquifer, m; K_{wi} is the water permeability in a radial section from r_i to r_{i+1}, *D*; Δp_i is the pressure drop in a radial section from r_i to r_{i+1}, kp_a; K_{w_avg} is the average water permeability over the rock section, *D*; *i* is the subsection index. The relative permeability concept to express water injectivity is as follows:

$$I_w = \frac{q_w}{\Delta p} = \frac{2 * 10^{-6} \pi h_w K K_{rw}}{\mu_w ln \frac{r_e}{r_w}} \tag{15}$$

where I_w is the water injectivity index, $m^3/s/kp_a$; q_w is the water injection rate, m^3/s; Δp is the pressure drop through the core, kp_a; K_w is the effective water permeability, *D*; *K* is the absolute permeability of the core, *D*; K_{rw} is the relative permeability to water, fraction; *h* is the length of injection completion, m; r_e is the radius of the aquifer, m. As only K_{rw} changes during the injection process, the water injectivity decline as a function of time can be calculated by the following equation:

$$I_D = \frac{K_{rw\_t}}{K_{rw\_0}} \tag{16}$$

where I_D is the dimensionless injectivity decline index, and subscripts 0 and *t* denote initial and instant values, respectively. Relative permeability values can be obtained in various ways. If core data are not available, Corey's function might approximate the relative permeability to water at different oil saturations as [48]:

$$\begin{cases} K_{rw} = K_{rw}^* \left(\frac{1 - S_o - S_{wc}}{1 - S_{wc} - S_{or}} \right)^{n_w} \\ K_{ro} = K_{ro}^* \left(\frac{S_o - S_{or}}{1 - S_{wc} - S_{or}} \right)^{n_o} \end{cases} \tag{17}$$

where K_{rw}^* is the water relative permeability at residual oil saturation, fraction; K_{ro}^* is the oil relative permeability at connate water saturation, fraction; S_{wc} is the connate water saturation, fraction; S_{or} is the residual oil saturation, fraction; n_w and n_o are the exponents for water and oil relative permeabilities, respectively, dimensionless. Thus, once the oil saturation is determined, the injectivity decline can be calculated.

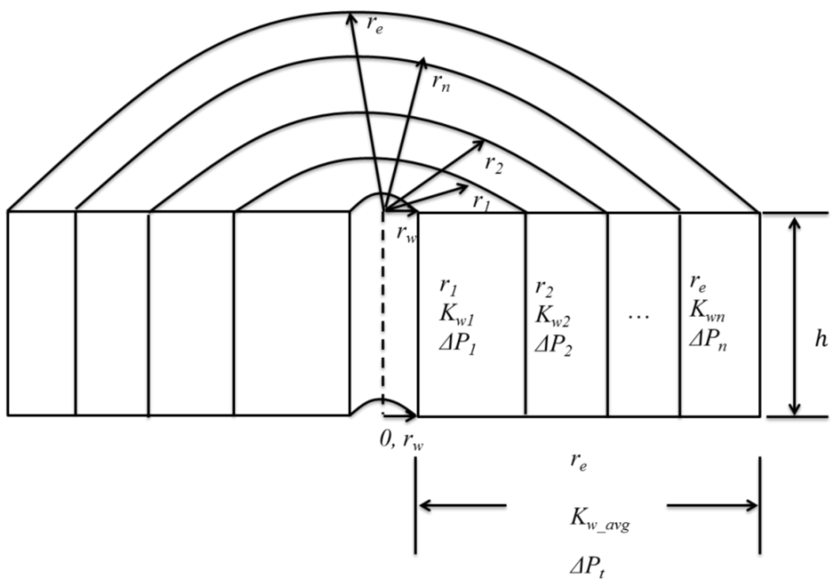

Figure 4. Local and average water permeability over the formation.

3.3. Skin Factor of Injectivity Decline

A skin factor has been used to describe the effects of formation permeability damage or stimulation around the wellbore for decades. It provides a convenient way to consider the effects of altered permeability in the formation near the wellbore. Considering the velocity change around the injection well, a radial composite model is used to describe the water permeability reduction effect in the near-wellbore region. The dynamic change of injectivity could be expressed in the following equation by including a skin factor:

$$I_w = \frac{2 * 10^{-6} \pi h_w K}{\mu_w \left(ln \frac{r_e}{r_w} + S \right)} \tag{18}$$

The oil saturation front moves forward with injection goes on, so the water permeability is assumed to be reduced from the original value K_{wi} to the skin permeability $K_{ws(t)}$ in a region from well radius r_w to the outer boundary of the permeability altered $r_{s(t)}$ at time t, where the dynamic skin factor is calculated as:

$$S(t) = \left(\frac{K_{wi}}{K_{ws(t)}} - 1 \right) ln \frac{r_{s(t)}}{r_w} \tag{19}$$

where subscript *(t)* means time t, K_{wi} is the original water permeability in each subsection from r_i to r_{i+1}, D; Δp_i is the pressure drop in each subsection if measurable; $r_{s(t)}$ is the radius of the oil invaded zone at time t, it is equal to the oil front position, m. The details of computing the oil front position and skin factor are described by Jin (2013) [40]. When the formation is damaged by oil, $K_{ws(t)}$ is smaller than K_{wi} and r_s increases with injection time. For an unfractured formation, the skin factor is always positive during the injection. Both experimental and simulation studies showed that the oil saturation front moves in the formation with a sharp interface [40–42]. Therefore, the radius of the skin zone is equal to the position of oil saturation front determined with the model, and skin permeability can be calculated using the following equation:

$$K_{ws\ (t)} = \frac{10^6 q \mu_w ln \frac{r_{s(t)}}{r_w}}{2\pi h_w} \frac{1}{\sum_{i=1}^{n} \Delta p_i} \tag{20}$$

By including the skin factor, the pressure drawdown required to maintain a constant injection rate is:

$$\Delta p_t = \frac{10^6 q \mu_w}{2\pi h_w K} \left[ln \frac{r_e}{r_w} + S(t) \right] \tag{21}$$

It is clear that higher pressure drawdown is required to inject the same amount of water when the skin factor increases, which means greater injection pressure is needed when the formation pressure is relatively stable, as shown in the following equation:

$$p_{r_w} = p_{r_e} + \frac{10^6 q \mu_w}{2\pi h_w K} \left[ln \frac{r_e}{r_w} + S(t) \right] \tag{22}$$

As the result, the pressure in the near-wellbore region will increase quickly with the rapid increase of skin factor when the injection water is contaminated by oil droplets. Using Equations (19) and (22), the relationship between injection rate, pressure, and time can be evaluated conveniently with the injectivity decline effect considered. A field case in the Gulf of Mexico showed that injection wells may require frequent stimulation to maintain the 7000 bpd (1113 m^3/d) injection rate in a formation where permeability is 1000 md and skin factor is 46 [49].

3.4. Geomechanical Model of Rock Failure

The potential risk of rock failure due to activation of slippage by water injection is analyzed here by considering weak planes' (joints) orientation and their strength in the rock and the in situ stress conditions. Different joints can be theoretically expected for different slip regimes. In a normal faulting regime, failure planes strike in the direction of maximum horizontal stress (SH) with dips comparable to the critical orientation. For the strike-slip faulting regime, the failure fractures will propagate in the vertical direction and strikes will generally bisect the SH and Sh (minimum horizontal stress) directions. Assuming joint planes are uniform and have preferred orientations for the rock failure is controlled by the required additional pore pressure for the slip of joints [50].

The Mohr-Coulomb failure criterion in Equation (1) is modified to investigate the failure of fractures as,

$$|\tau| = \tau_s + \sigma_n{}' \tan \varphi' \tag{23}$$

where τ is the shear stress, τ_s is the shear strength or cohesive strength, $\sigma_n{}'$ is the effective normal stress and φ' is the joint friction angle.

In Equation (23), the effective normal stress, σ_n, and shear stress, τ, on the planes of weakness can be calculated by the following equations:

$$\begin{gathered} \sigma_n = l^2\sigma_1 + m^2\sigma_2 + n^2\sigma_3 \\ \tau = \sqrt{l^2m^2(\sigma_1 - \sigma_2)^2 + n^2m^2(\sigma_3 - \sigma_2)^2 + l^2n^2(\sigma_3 - \sigma_1)^2} \end{gathered} \tag{24}$$

where l, m, and n are direction cosines of the angles between normal to a given plane to the direction of three arbitrarily assumed principal stresses (σ_1, σ_2, σ_3). In the case when the three stresses are defined as vertical stress, σ_v, maximum horizontal stress, $\sigma_{\boldsymbol{H}}$, and minimum horizontal stress, σ_h, the model in Equation (24) can be simplified by substituting (σ_v, σ_H, σ_h) for (σ_1, σ_2, σ_3). Additionally, in such a case, the values of l, m, and n in Equation (24) become equal to the values of direction cosines of the angles between normal to the weakness plane and the direction of vertical and horizontal stresses (d_H, d_h, and d_v) as,

$$\begin{gathered} d_H = \cos(90 - \delta) \times \cos(90 - \varphi) \\ d_h = \cos(90 - \delta) \times \sin(90 - \varphi) \\ d_v = \sin(90 - \delta) \end{gathered} \tag{25}$$

where δ is the dip angle and φ is the dip direction angle. The above simplification is not accurate, as we know, especially in the mountain areas. However, it could be acceptable for geological subsurface in the Great Plains area.

Using the failure criterion and the orientations of joints, a slippage diagram can be made to determine values of additional pore pressure needed for reactivation slippage along the weak interfaces considering their various positions (dip and azimuth angles). An example slippage diagram for the Entrada formation is shown in Figure 5 using data in Table A1. The diagram's concentric circles correspond to the dip angle of joints with zero value in the center and 90 degrees at the outer circle. The radial dashed lines represent the azimuth normal to the weak interface. More details about the calculation and construction of slippage diagrams can be found in Ge and Ghassemi (2012) [50].

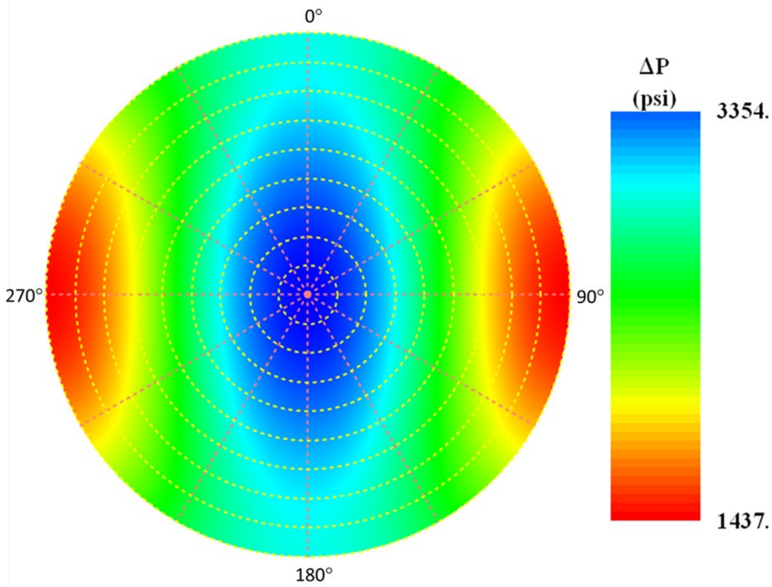

Figure 5. Additional pore pressure for shear slippage in Entrada formation (3554 psi = 23,125 KPa, 1437 psi = 9908 KPa).

In the example diagram in Figure 5 fractures in the W-E direction and with high dip angles are easier to reactivate (lower pressure increase is needed) and cause seismicity, while fractures in the N-S direction would be more stable. Specifically, the slippage diagram in Figure 5 shows that for an injection well in the Entrada formation the highest values of pore pressure increase (due injection) are needed for reactivation of interfaces that are close to horizontal (blue area) while strike-slippage of a vertical fault could occur at very low injection pressure when the fault face is in W-E direction. Moreover, if such a fault happens to be very close to the injection well its slippage (and resulting seismic event) would occur at a pressure much lower than the wellbore fracturing pressure (1437 < 4434 psi [9908 < 30,571 KPa]).

In all, when the stress conditions and fracture orientations in the injected formation are known, operators could use slippage diagrams to estimate critical pore pressure and further decide on the injection pressures and rates for their PWRI operations to avoid fracture reactivation and induced seismicity.

4. Case Study

Three formations with different rock and fluid properties are selected to investigate the oily water injection behavior and to identify the critical injection rate for preventing rock failure caused by fracturing, i.e., the Type I rock failure. The formations are in the actual oilfields with water production and injection operations. With different reservoir and fluid properties, the formations cover a wide range of real-world scenarios.

Table A1 shows the fluids and rock properties of an aquifer for produced water re-injection in the Entrada formation in New Mexico. The permeability of the formation is 256 mD (2.5×10^{-13} m^2) in the studied area and the formation fracturing pressure is 4334 psi (29,882 KPa). Figures 6 and 7 show the skin factor and injection pressure increase during the injection process, respectively, which can be used to design safe injection operations. Due to the low oil concentration (500 ppm) in the injection water, the overall skin factor is small–less than 2.5 when the injection rate is below 10,000 bpd (1590 m^3/d). However, even such a small skin factor could cause formation damage due to the low absolute permeability and water-wet characteristic of the formation. The injection pressure reaches the fracturing pressure in 5 days at an injection rate of 5000 bpd (795 m^3/d), and a 10,000 bpd (1590 m^3/d) injection rate will cause formation failure immediately, as shown in Figure 7. However, the formation will not be fractured for a long time when the injection rate is 2000 bpd.

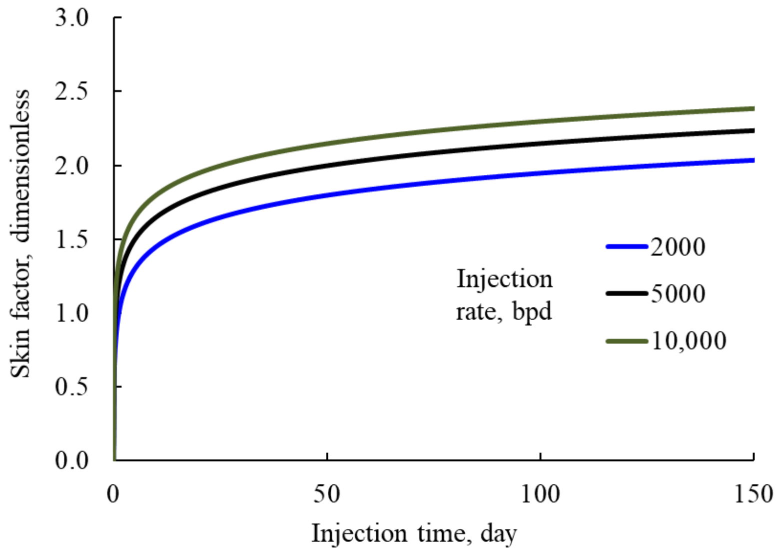

Figure 6. The skin factor develops with time for different injection rates (2000–10,000 bpd [318–1590 m^3/d]) in Entrada formation.

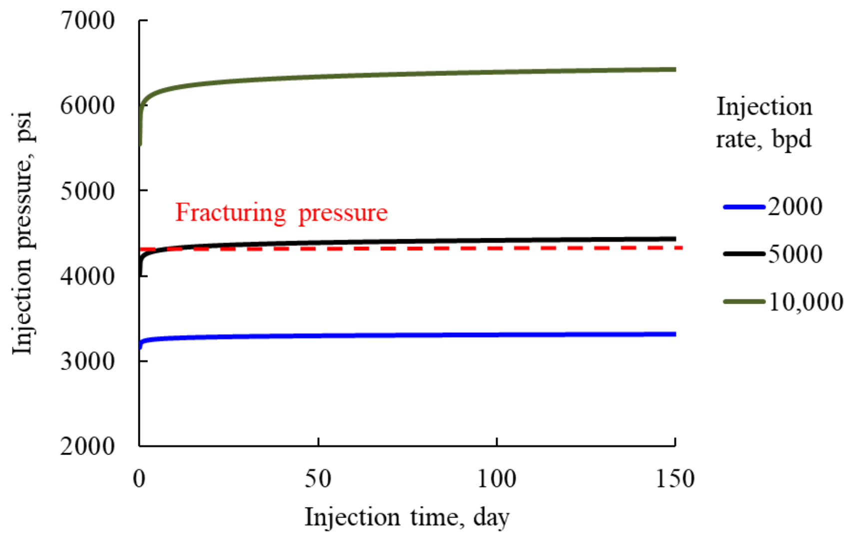

Figure 7. Injection pressure increases with time for different injection rates (2000–10,000 bpd [318–1590 m^3/d]) in Entrada formation. The horizontal red dash line is the fracturing pressure in the reservoir. (Pressure scale in the figure: 2000–7000 psi [13,790–48,263 KPa]).

For some formations with low permeability, even a small injection rate could trigger seismic activity because the injection pressure could easily exceed the critical pressure and cause rock failure. For example, based on the reservoir and fluid data for the Entrada formation, if a location has a permeability of 25 mD (2.5×10^{-14} m^2), the bottomhole pressure would reach the critical injection pressure causing formation fracturing in just one month with an injection rate of 300 bpd (48 m^3/d), as shown in in Figure 8.

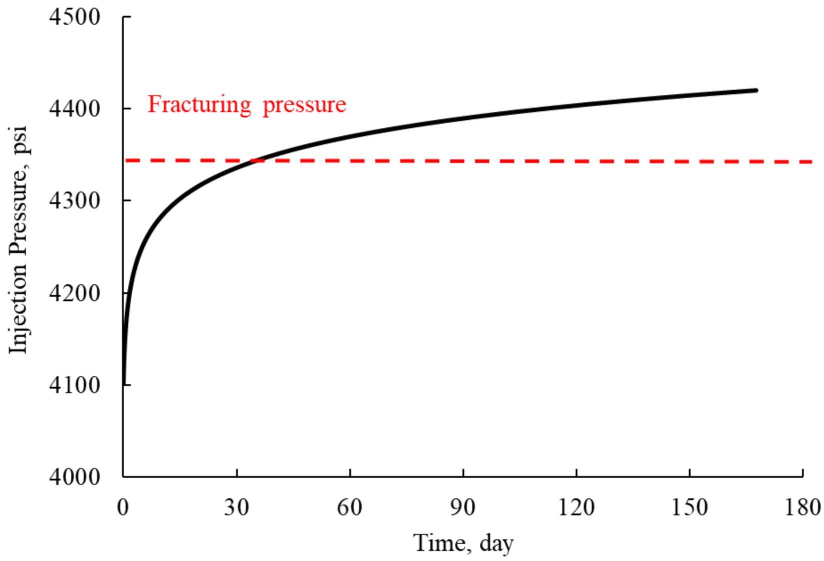

Figure 8. Wastewater injection could trigger rock failure in a low-permeability location at the Entrada Formation (k = 25 md [2.5×10^{-14} m^2], q_w = 300 bpd [48 m^3/d]). The horizontal red dash line is the fracturing pressure in the reservoir. (Pressure scale in the figure: 4000–4500 psi [27,579–31,026 KPa]).

The M field is a shallow heavy oil field with thick bottom water located on the west coast of Africa. The fluid and rock properties of the field are shown in Table A2. The reservoir has a moderate permeability (1218 mD [1.2×10^{-12} m^2]) and a critical pressure of 986 psi (6798 KPa). Due to the high oil viscosity and thick aquifer, a large volume of produced water needs to be disposed of for economic oil production. The injection pressure is shown in Figure 9 when water is injected from 2000 to 7000 bpd (318–1113 m^3/d) with 500 ppm oil. The results indicate that water can be injected safely below 5000 bpd (795 m^3/d) without stimulation for more than 500 days. However, when the injection rate increases to 6000 bpd (954 m^3/d), the formation needs to be stimulated at 280 days and the stimulation cycle reduces to 75 days if the injection rate increases to 7000 bpd (1113 m^3/d). Due to the shallow depth of the reservoir, the rock may fail in the reservoir if the water injection is not properly designed.

The Nebo-Hemphill field in North Louisiana is a bottom-water-drive reservoir with active water coning. To control this problem, downhole water sink (DWS) technology was used and good results were reported [51,52]. However, due to the strong water coning, water needs to be drained at a rate of 2000 to 5000 bpd (318 to 795 m^3/d) to reduce water cut in the production stream. Since there is a thick aquifer with high permeability (3500 mD [3.5×10^{-12} m^2]) under the oil zone as shown in Table A3, the produced water could be injected back into the aquifer for pressure maintenance and water coning control purposes. The critical pressure for this reservoir is 1466 psi (10,108 KPa). If the injection water contains 500 ppm oil and is injected from 2000 to 5000 bpd (318 to 795 m^3/d), then the injection pressure can be calculated as shown in Figure 10. The results show that oily water can be safely injected into the aquifer without fracturing the formation even if the injection rate reaches 5000 bpd (795 m^3/d), and the formation does not need to be stimulated for a long time due to the high absolute permeability.

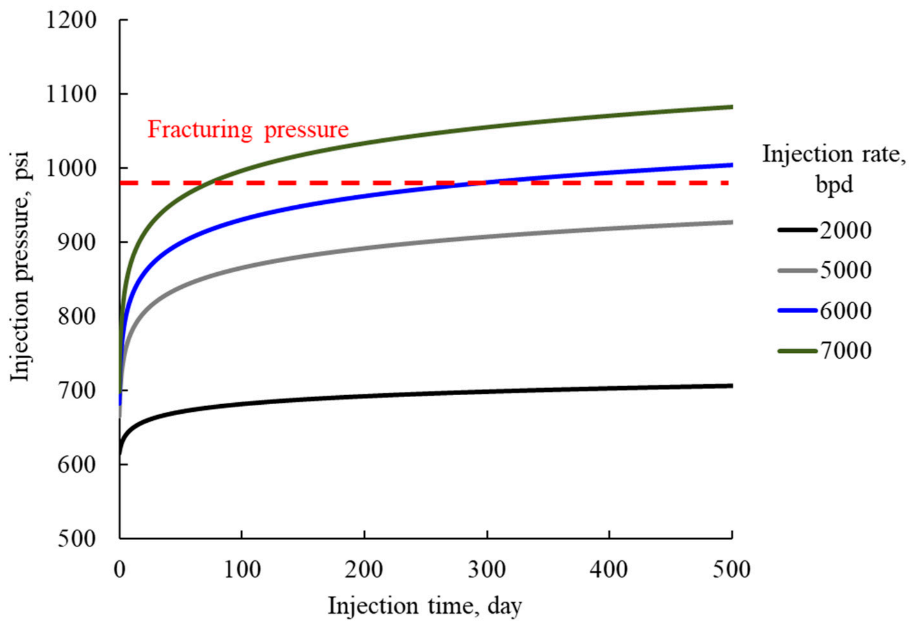

Figure 9. Evaluation of water injection at different rates (2000–7000 bpd [318–1113 m^3/d]) in the M field. The horizontal red dash line is the fracturing pressure in the reservoir. (Pressure scale in the figure: 500–1200 psi [3447–8274 KPa]).

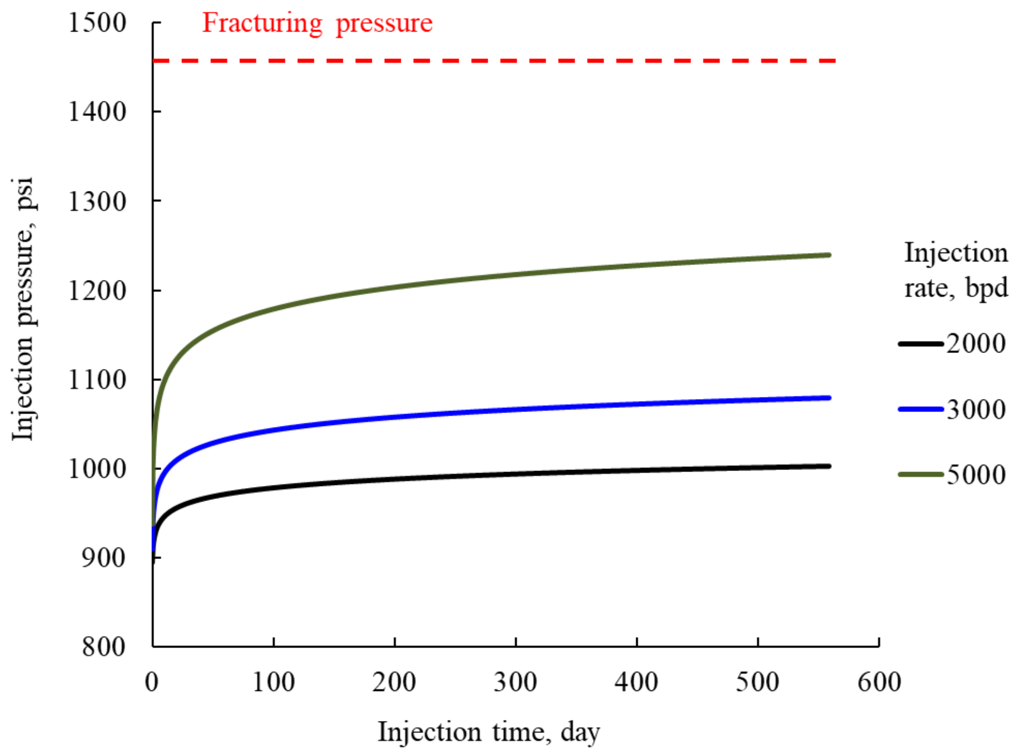

Figure 10. Evaluation of water injection at different rates (2000–5000 bpd [318–795 m^3/d]) in the Nebo-Hemphill field. The horizontal red dash line is the fracturing pressure in the reservoir. (Pressure scale in the figure: 800–1500 psi [5516–10,342 KPa]).

5. Discussion

The methodology introduced in this paper contributes to the design of produced water injection wells operation by including oil contamination as an additional design parameter. The study also formulates an additional component of environmental risk of Class II injection wells by defining seismicity as another environmental risk criterion to the regulatory-promulgated standard of groundwater contamination.

Moreover, the study attempts to quantify the new criterion in terms of fracturing the injection zone or reactivation of strained interfaces within the zone. It also explains why there are no seismic events in areas with low water injection rates, highly permeable, strong, and regular sediments, while other areas with a high volume of injected water into weak low-permeability strata with complex tectonics are likely to have frequent earthquakes. Specifically, the effect of excessive injection rate has been already confirmed in the field operations in Barnett Shale where wells located in the areas with recorded frequent earthquakes injected water at rates exceeding 150,000 barrels/month (23,848 m^3/month) [18].

The study only considers the scenario of a seismic event occurring in the injection well's vicinity when the well's pressure exceeds either formation fracture pressure or critical pore pressure for shear failure at the rock's weak interface (fault or joint surface). However, reported earthquakes have been observed close to the injectors shortly after the injection began as well as away from the injection wells–after many years of injection. Depending on the distance between the injector and fault, it may take more time for the fault to be activated by pressure from a distant injector. Therefore, there is a need to extend the injection pressure model presented in this study (based upon time-related skin factor) by considering spatial expansion of the high-pressure zone resulting from progressive capture of oil in the rock away from the well (based upon skin factor vs. time and radius).

Based on the three cases studied above, it is clear that water injection rate, formation permeability, and critical (fracturing) pressure play important roles in induced seismic events. However, the studies assume the priority of rock fracturing events over pore-pressure-induced slippage that may not always be the case–particularly when the injection well is drilled close to the fault. Thus, there is a need for more field data on geostatic stresses from injection areas rather than shale-fracturing operations reported here.

The proposed hydraulic model of well injectivity loss fully explains the rapid increase of injection pressure resulting from oil capture around the well. The results confirm field observations relating more frequent well stimulations to the level of oil contamination of re-injected produced water. However, the geomechanical model of rock failure does not consider the effect of captured oil on the angle of internal friction of the rock and at the rock slippage interface. This "oil lubrication" effect may strongly reduce the value of critical pore pressure.

6. Conclusions

To assess the environmental risk of inducing seismic events by an injection well, we consider a formation permeability damage caused by invasion and capture of the water-contaminating oil and a mechanical damage of formation resulting from hydraulic fracturing and/or internal shear failure during PWRI. A seismic event occurs when the pressure caused by permeability damage exceeds formation strength leading to mechanical damage.

The proposed analytical model of formation permeability damage employs the theory of two-phase radial flow and retention of oil droplets in porous media to predict the time and distance-based oil saturation, relative permeability, and pressure in the formation. In this study, the model is simplified by computing the overall skin factor to determine the pressure at the well's bottom.

Formation mechanical damage is modeled using either the concept of exceeding the hoop stress around the wellbore and hydraulic fracturing or exceeding the formation pore pressure and slippage within the rock structure. The two models are tested using data from three geological formations in areas of petroleum operations. The following conclusions are drawn from the study:

1. All the studies show that injection of oily water would cause a rapid initial increase of pressure due well's injectivity decline when an equilibrium oil saturation develops in the near-wellbore region. In the Entrada formation, even a low oil concentration of 500 ppm in the injection water would generate a positive skin factor in less than 30 days;

2. The strong effect of excessive oil concentration on early pressure increase could only be controlled by reducing the rate of injection to assure continuing long-time operation as is the case in the M field. This may be important in designing a water disposal system in oilfields with a large volume of produced water where the number and cost of designated injection wells have to be weighed against the frequency (and cost) of well stimulations needed to control injectivity damage;
3. Formations with high initial permeability (>3000 mD [3.0×10^{-12} m^2]) are favorable for oily water injection. A loss of 30% water injectivity caused by oily water injection may not harm the overall injection performance;
4. Water injection is not likely to induce seismic events when the injected formation has high permeability and high fracturing pressure, especially when injectors are far away from faults. However, for formations with low permeability (<25 mD [2.5×10^{-14} m^2]) assuming the other properties are the same as shown in Table A1 even a small injection rate (300 bpd [48 m^3/d]) could trigger a series of seismic events string with rock fracture due to rapid injection pressure increase in the near-wellbore region and possibly followed by slippage of the nearby fault or unstable strike-slip rock structure.
5. The case studies show different long-time patterns of injection pressure increase: a flat pattern with practically no pressure increase in the Entrada formation, and a progressive–pattern with continuous pressure increase in the M and the Nebo-Hemphill oilfields–particularly at higher injection rates. The two patterns may result from different mechanisms of oil capture inside the rock with the flat pattern representing local near-well permeability damage due to local oil capture, and the progressive pattern indicating radial expansion of oil capture–as implied by Equation (20).

Author Contributions: Conceptualization and flow modeling, L.J. and A.K.W.; geologic modeling, J.G. All authors have read and agreed to the published version of the manuscript.

Funding: This research was funded by the LSU Downhole Water Sink Technology Initiative (DWSTI) and APC was paid by Louisiana State University.

Data Availability Statement: The field data used in this study was provided by the LSU Downhole Water Sink Technology Initiative (DWSTI). The source data can be found in the corresponding author's Ph. D dissertation "Jin, L. A Feasibility Study of Multi-Functional Wells for Water Coning Control and Disposal. Ph. D dissertation, Louisiana State University, Baton Rouge, LA, December 2013" [40].

Acknowledgments: The authors would like to express their gratitude to the LSU Downhole Water Sink Technology Initiative (DWSTI) for supporting this research. We also would like to thank the partner companies for allowing us to publish the field data. Part of the research content was adopted from the corresponding author's Ph. D dissertation "Jin, L. A Feasibility Study of Multi-Functional Wells for Water Coning Control and Disposal. Ph. D dissertation, Louisiana State University, Baton Rouge, LA, December 2013.", and part of the technical content was presented in the SPE Health, Safety, Security, Environment & Social Responsibility Conference-North America, New Orleans, LA, 18–20 April 2017.

Conflicts of Interest: The authors declare no conflict of interest.

Appendix A. Field Data for Case Study

Table A1. Properties of the Entrada formation in New Mexico [40].

Parameter	Value	Unit	Value	Unit
Water injection rate (q)	2000~10,000	bpd	318~1590	m^3/d
Absolute permeability (K)	256	mD	2.5×10^{-13}	m^2
Porosity (ϕ)	0.212	fraction	0.212	fraction
Well radius (r_w)	0.292	ft	0.089002	m
Formation radius (r_e)	1000	ft	304.8	m
Formation depth (H_a)	5914	ft	1797	m
Formation thickness (h_w)	15	ft	4.572	m
Formation pressure (p_{r_e})	2560	psi	17,656	kp_a
Formation fracturing pressure (p_f)	4334	psi	29,882	kp_a
Oil density (ρ_o)	7.18	lbm/ft^3	860	kg/m^3
Water viscosity (μ_w)	1	cp	1	cp
Oil viscosity (μ_o)	6.11	cp	6.11	cp
Water relative permeability exponent (n_w)	4	dimensionless	4	dimensionless
Oil relative permeability exponent (n_o)	6	dimensionless	6	dimensionless
Connate water saturation (S_{wc})	0.068	fraction	0.068	fraction
Residual oil saturation (S_{or})	0	fraction	0	fraction
Oil concentration (C_0)	500	ppm	500	ppm
Equilibrium oil saturation (S_{oe})	0.08	fraction	0.08	fraction
Oil-water interfacial tension (σ_{ow})	35	dyne/cm	35	dyne/cm
Critical capillary number (N_{Ca}^*)	10^{-4}	dimensionless	10^{-4}	dimensionless
Bump rate constant (λ)	5	dimensionless	5	dimensionless
Size ratio (N_d)	0.152	dimensionless	0.152	dimensionless
Poison's Ratio (v)	0.311	dimensionless	0.311	dimensionless
Vertical principal stress	5914	psi	40,775	kPa
Horizontal maximum principal stress	5396	psi	37,204	kPa
Horizontal minimumprincipal stress	3997	psi	27,558	kPa
Cohesion (τ_0)	1200	psi	8273	kPa
Friction coefficient (μ_f)	0.6	dimensionless	0.6	dimensionless

Table A2. Properties of the M field in the west coast of Africa [40].

Parameter	Value	Unit	Value	Unit
Water injection rate (q)	2000~7000	bpd	318–1113	m^3/d
Absolute permeability (K)	1218	mD	1.2×10^{-12}	m^2
Porosity (ϕ)	0.28	fraction	0.28	fraction
Well radius (r_w)	0.292	ft	0.089002	m
Oil zone thickness (h_o)	65.6	ft	20	m
Aquifer radius (r_e)	1000	ft	304.8	m
Aquifer depth (H_a)	1345	ft	410	m
Aquifer thickness (h_w)	295	ft	90	m
Drainage completion length (h_{wd})	20	ft	6	m

Table A2. *Cont.*

Parameter	Value	Unit	Value	Unit
Injection completion length (h_{wi})	20	ft	6	m
Aquifer outer boundary pressure (p_{r_e})	582.5	psi	4016	kpa
Formation fracturing pressure (p_f)	986	psi	6798	kpa
Oil density (ρ_o)	58.68	lbm/ft^3	940	kg/m^3
Water viscosity (μ_w)	0.7	cp	0.7	cp
Oil viscosity (μ_o)	230	cp	230	cp
Water relative permeability exponent (n_w)	7	dimensionless	7	dimensionless
Oil relative permeability exponent (n_o)	5	dimensionless	5	dimensionless
Connate water saturation (S_{wc})	0.224	fraction	0.224	fraction
Residual oil saturation (S_{or})	0	fraction	0	fraction
Oil concentration (C_0)	500	ppm	500	ppm
Equilibrium oil saturation (S_{oe}^*)	0.34	fraction	0.34	fraction
Oil-water interfacial tension (σ_{ow})	50	dyne/cm	50	dyne/cm
Critical capillary number (N_{Ca}^*)	10^{-4}	dimensionless	10^{-4}	dimensionless
Bump rate constant (λ)	5	dimensionless	5	dimensionless
Size ratio (N_d)	0.5	dimensionless	0.5	dimensionless

Table A3. Properties of the Nebo-Hemphill field in North Louisiana [40].

Parameter	Value	Unit	Value	Unit
Water injection rate (q)	2000~5000	bpd	318–795	m^3/d
Absolute permeability (K)	3500	mD	3.5×10^{-12}	m^2
Porosity (ϕ)	0.3	fraction	0.3	fraction
Well radius (r_w)	0.292	ft	0.089002	m
Oil zone thickness (h_o)	18	ft	5.486	m
Aquifer radius (r_e)	850	ft	259	m
Aquifer depth (H_a)	2000	ft	607.6	m
Aquifer thickness (h_w)	64	ft	19.5	m
Drainage completion length (h_{wd})	12	ft	3.66	m
Injection completion length (h_{wi})	12	ft	3.66	m
Aquifer outer boundary pressure (p_{r_e})	866	psi	5971	kpa
Formation fracturing pressure $\left(p_f\right)$	1466	psi	10108	kpa
Oil density (ρ_o)	58.058	lbm/ft^3	930	kg/m^3
Water viscosity (μ_w)	1	cp	1	cp
Oil viscosity (μ_o)	17	cp	17	cp
Water relative permeability exponent (n_w)	7	dimensionless	7	dimensionless
Oil relative permeability exponent (n_o)	4	dimensionless	4	dimensionless
Connate water saturation in aquifer (S_{wc})	0.2	fraction	0.2	fraction
Residual oil saturation in aquifer (S_{or})	0	fraction	0	fraction
Oil concentration (C_0)	500	ppm	500	ppm
Equilibrium oil saturation (S_{oe}^*)	0.29	fraction	0.29	fraction

Table A3. *Cont.*

Parameter	Value	Unit	Value	Unit
Oil-water interfacial tension (σ_{ow})	30	dyne/cm	30	dyne/cm
Critical capillary number (N^*_{Ca})	10^{-4}	dimensionless	10^{-4}	dimensionless
Bump rate constant (λ)	5	dimensionless	5	dimensionless
Size ratio (N_d)	0.4	dimensionless	0.4	dimensionless

References

1. Al-Ghouti, M.A.; Al-Kaabi, M.A.; Ashfaq, M.Y.; Da'na, D.A. Produced water characteristics, treatment and reuse: A review. *J. Water Process Eng.* **2019**, *28*, 222–239. [CrossRef]
2. Veil, J.U.S. Produced Water Volumes and Management Practices in 2017. February 2020. Report for Ground Water Protection Council (GWPC). Available online: https://www.gwpc.org/sites/gwpc/uploads/documents/publications/pw_report_2017___final.pdf (accessed on 5 February 2022).
3. Horner, R.M.; Harto, C.B.; Jackson, R.B.; Lowry, E.R.; Brandt, A.R.; Yeskoo, T.W.; Murphy, D.J.; Clark, C.E. Water Use and Management in the Bakken Shale Oil Play in North Dakota. *Environ. Sci. Technol.* **2016**, *50*, 3275–3282. [CrossRef] [PubMed]
4. Jin, L.; Wojtanowicz, A.K.; Ge, J. An Analytical Model Predicts Pressure Increase during Waste Water Injection to Prevent Fracturing and Seismic Events. In Proceedings of the SPE Health, Safety, Security, Environment, & Social Responsibility Conference-North America, New Orleans, LA, USA, 18–20 April 2017.
5. Kondash, A.J.; Lauer, N.E.; Vengosh, A. The intensification of the water footprint of hydraulic fracturing. *Sci. Adv.* **2018**, *4*, eaar5982. [CrossRef] [PubMed]
6. U.S. Environmental Protection Agency. EPA Hydraulic Fracturing Study Technical Workshop #4. Available online: https://www.epa.gov/sites/default/files/documents/09_Mantell_-_Reuse_508.pdf (accessed on 5 February 2022).
7. Jin, L.; Wojtanowicz, A.K.; Hughes, R.G. An Analytical Model for Water Coning Control Installation in Reservoir with Bottomwater. *J. Can. Pet. Technol.* **2010**, *49*, 65–70. [CrossRef]
8. Jin, L.; Wojtanowicz, A.K. Performance Analysis of Wells with Downhole Water Loop Installation for Water Coning Control. *J. Can. Pet. Technol.* **2010**, *49*, 38–45. [CrossRef]
9. Jin, L.; Wojtanowicz, A.K. Minimum Produced Water from Oil Wells with Water-Coning Control and Water-Loop Installations. In Proceedings of the SPE Americas E&P Health, Safety, Security, and Environmental Conference, Houston, TX, USA, 21–23 March 2011. SPE 143715.
10. Scanlon, B.R.; Reedy, R.C.; Male, F.; Walsh, M. Water Issues Related to Transitioning from Conventional to Unconventional Oil Production in the Permian Basin. *Environ. Sci. Technol.* **2017**, *51*, 10903–10912. [CrossRef] [PubMed]
11. Pena Castro, A.F.; Dougherty, S.L.; Harrington, R.M.; Cochran, E.S. Delayed dynamic triggering of disposal-induced earthquakes observed by a dense array in northern Oklahoma. *J. Geophys. Res. Solid Earth* **2019**, *124*, 3766–3781. [CrossRef]
12. Horton, S. Disposal of Hydrofracking Waste Fluid by Injection into Subsurface Aquifers Triggers Earthquake Swarm in Central Arkansas with Potential for Damaging Earthquake. *Seismol. Res. Lett.* **2012**, *83*, 250–260. [CrossRef]
13. Davis, S.D.; Frohlich, C. Did (Or Will) Fluid Injection Cause Earthquakes?—Criteria for a Rational Assessment. *Seismol. Res. Lett.* **1993**, *64*, 207–224. [CrossRef]
14. Rubinstein, J.L.; Mahani, A.B. Myths and Facts on Wastewater Injection, Hydraulic Fracturing, Enhanced Oil Recovery, and Induced Seismicity. *Seismol. Res. Lett.* **2015**, *86*, 1060–1067. [CrossRef]
15. USGS. Induced Earthquakes. Available online: https://www.usgs.gov/programs/earthquake-hazards/induced-earthquakes (accessed on 18 December 2021).
16. McGarr, A.; Bekins, B.; Burkardt, N.; Dewey, J.; Earle, P.; Ellsworth, W.; Ge, S.; Hickman, S.; Holland, A.; Majer, E.; et al. Coping with Earthquakes Induced by Fluid Injection. *Science* **2015**, *347*, 830–831. [CrossRef] [PubMed]
17. Wang, K.; Ellsworth, W.; Beroza, G.C. Revisiting the Timpson Induced Earthquake Sequence: A System of Two Parallel Faults. *Geophys. Res. Lett.* **2020**, *47*, e2020GL089192. [CrossRef]
18. Frohlich, C. Two-year survey comparing earthquake activity and injection-well locations in the Barnett Shale, Texas. *Proc. Natl. Acad. Sci. USA* **2012**, *109*, 13934–13938. [CrossRef]
19. Folger, P.; Tiemann, M. *Human-Induced Earthquakes from Deep-Well Injection: A Brief Overview*; Congressional Research Service: Washington, DC, USA, 2014.
20. Van der Zwaag, C.; Øyno, L. Comparison of Injectivity Prediction Models to Estimate Ula Field Injector Performance for Produced Water Reinjection. *Environ. Sci. Res.* **1996**, *52*, 521–532. Available online: https://jglobal.jst.go.jp/en/detail?JGLOBAL_ID=200902161456566079 (accessed on 29 December 2021).
21. Underground Injection Control Program. Available online: https://www.ecfr.gov/current/title-40/chapter-I/subchapter-D/part-144 (accessed on 5 February 2022).
22. Lund Snee, J.E.; Zoback, M.D. Multiscale variations of the crustal stress field throughout North America. *Nat. Commun.* **2020**, *11*, 1951. [CrossRef]

23. Obe, I.; Fashanu, T.A.; Idialu, P.O.; Akintola, T.O.; Abhulimen, K.E. Produced water re-injection in a non-fresh water aquifer with geochemical reaction, hydrodynamic molecular dispersion and adsorption kinetics controlling: Model development and numerical simulation. *Appl. Water Sci.* **2017**, *7*, 1169–1189. [CrossRef]
24. Cox, S. The application of failure mode diagrams for exploring the roles of fluid pressure and stress states in controlling styles of fracture-controlled permeability enhancement in faults and shear zones. *Geofluids* **2010**, *10*, 217–233.
25. Dvory, N.Z.; Zoback, M.D. Assessing Fault Slip Potential in A Continuously Varying Stress Field–Application in the Delaware Basin. In Proceedings of the 55th US Rock Mechanics/Geomechanics Symposium, Online, 18–21 June 2021.
26. Alhosani, A.; Scanziani, A.; Lin, Q.; Foroughi, S.; Alhammadi, A.M.; Blunt, M.J.; Bijeljic, B. Dynamics of water injection in an oil-wet reservoir rock at subsurface conditions: Invasion patterns and pore-filling events. *Phys. Rev. E* **2020**, *102*, 023110. [CrossRef] [PubMed]
27. Mathias, S.A.; De Miguel, G.J.G.M.; Thatcher, K.E.; Zimmerman, R.W. Pressure Buildup During CO2 Injection into a Closed Brine Aquifer. *Transp. Porous Media* **2011**, *89*, 383–397. [CrossRef]
28. Mathias, S.A.; McElwaine, J.N.; Gluyas, J.G. Heat transport and pressure buildup during carbon dioxide injection into depleted gas reservoirs. *J. Fluid Mech.* **2014**, *756*, 89–109. [CrossRef]
29. Noirot, J.C.; Van den Hoek, P.J.; Zwarts, D.; Bjoerndal, H.P.; Stewart, G.; Drenth, R.; Al-Masfry, R.; Was-sing, B.; Saeby, J.; Al-Masroori, M.; et al. Water injection and water flooding under fracturing conditions. In Proceedings of the Middle East Oil Show, Manama, Bahrain, 9–12 June 2003.
30. Lyu, W.; Zeng, L.; Chen, M.; Qiao, D.; Fan, J.; Xia, D. An approach for determining the water injection pressure of low-permeability reservoirs. *Energy Explor. Exploit.* **2018**, *36*, 1210–1228. [CrossRef]
31. Abbaszadeh, M.; Kamal, M. Pressure-Transient Testing of Water-Injection Wells. *SPE Reserv. Eng.* **1989**, *4*, 115–124. [CrossRef]
32. Coulibaly, K.M.; Borden, R.C. Impact of edible oil injection on the permeability of aquifer sands. *J. Contam. Hydrol.* **2004**, *71*, 219–237. [CrossRef] [PubMed]
33. Khan, N.A.; Engle, M.; Dungan, B.; Holguin, F.; Xu, P.; Carroll, K.C. Volatile-organic molecular characterization of shale-oil produced water from the Permian Basin. *Chemosphere* **2016**, *148*, 126–136. [CrossRef]
34. Ohen, H.A.; Nnabuihe, L.; Felber, B.J.; Ososanwo, D.; Holmgren, C.M. A Systematic Laboratory Core and Fluid Analysis Program for the Design of a Cost-Effective Treatment and Cleanup Guidelines for a Produced Water Disposal Scheme. In Proceedings of the SPE/DOE Improved Oil Recovery Symposium, Tulsa, OK, USA, 21–24 April 1996. SPE 35369.
35. Veil, J.A.; Quinn, J.J. *Downhole Separation Technology Performance: Relationship to Geologic Condition*; Report for U.S. DOE; National Energy Technology Laboratory: Pittsburgh, PA, USA, 2004.
36. Palsson, B.; Davies, D.R.; Todd, A.C.; Somerville, J.M. The Water Injection Process A Technical and Economic Integrated Approach. *Chem. Eng. Res. Des.* **2003**, *81 Pt A*, 333–341. [CrossRef]
37. Bennion, D.; Thomas, F.; Bietz, R. Injection Water Quality-A Key Factor to Successful Waterflooding. *J. Can. Pet. Technol.* **1998**, *37*, 53–62. [CrossRef]
38. Nicholson, C.; Wesson, R.L. *Earthquake Hazard Associated with Deep Well Injection: A Report to the U.S. Environmental Protection Agency*; U.S. Geological Survey: Reston, VA, USA, 1990; Volume 1951.
39. Jin, L.; Wojtanowicz, A. Experimental and theoretical study of counter-current oil–water separation in wells with in-situ water injection. *J. Pet. Sci. Eng.* **2013**, *109*, 250–259. [CrossRef]
40. Jin, L. A Feasibility Study of Multi-Functional Wells for Water Coning Control and Disposal. Ph.D. Dissertation, Louisiana State University, Baton Rouge, LA, USA, December 2013.
41. Soo, H.; Radke, C.J. Flow mechanism of dilute, stable emulsions in porous media. *Ind. Eng. Chem. Fundam.* **1984**, *23*, 342–347. [CrossRef]
42. Soo, H.; Williams, M.; Radke, C. A filtration model for the flow of dilute, stable emulsions in porous media—II. Parameter evaluation and estimation. *Chem. Eng. Sci.* **1986**, *41*, 273–281. [CrossRef]
43. Jin, L.; Wojtanowicz, A.K. Development of Injectivity Damage due Oily Waste Water in Linear Flow. In Proceedings of the SPE International Symposium and Exhibition on Formation Damage Control, Lafayette, LA, USA, 26–28 February 2014. SPE 168130.
44. Jin, L.; Wojtanowicz, A.K. Progression of injectivity damage with oily waste water in linear flow. *Pet. Sci.* **2014**, *11*, 550–562. [CrossRef]
45. Bear, J. *Dynamics of Fluids in Porous Media*; Elsevier Publishing Co., Inc.: New York, NY, USA, 1972; pp. 665–727.
46. Lake, L.W. *Enhanced Oil Recovery*; Prentice Hall: Hoboken, NJ, USA, 1989.
47. Saripalli, K.; Sharma, M.; Bryant, S. Modeling injection well performance during deep-well injection of liquid wastes. *J. Hydrol.* **2000**, *227*, 41–55. [CrossRef]
48. Brooks, R.H.; Corey, A.T. Properties of Porous Media Affecting Fluid Flow. *J. Irrig. Drain. Div.* **1966**, *92*, 61–88. [CrossRef]
49. Sharma, M.M.; Pang, S.; Wennberg, K.E.; Morgenthaler, L.N. *Injectivity Decline in Water-Injection Wells: An Offshore Gulf of Mexico Case Study*; SPE Production & Facilities: Richardson, TX, USA, 2000; Volume 15.
50. Ge, J.; Ghassemi, A. Stimulated Reservoir Volume by Hydraulic Fracturing in Naturally Fractured Shale Gas Reservoirs. In Proceedings of the 46th U.S. Rock Mechanics Symposium, Chicago, IL, USA, 24–27 June 2012.

51. Swisher, M.D.; Wojtanowicz, A.K. New Dual Completion Method Eliminates Bottom Water Coning. In Proceedings of the SPE ATCE, Dallas, TX, USA, 22–25 October 1995; SPE 30697.
52. Swisher, M.; Wojtanowicz, A. In Situ-Segregated Production of Oil and Water—A Production Method with Environmental Merit: Field Application. *SPE Adv. Technol. Ser.* **1996**, *4*, 51–58. [CrossRef]